Biomedical Spectroscopy and Imaging 4 (2015) 95–103
DOI 10.3233/BSI-140100
IOS Press

Morphological, plasmonic and SERS characterization of DC-sputtered gold nanoislands

Ji Qi [a], Pratik Motwani [a], Jianbo Zeng [a], John C. Wolfe [a] and Wei-Chuan Shih [a,b,*]
[a] *Department of Electrical & Computer Engineering, University of Houston, Houston, TX, USA*
[b] *Department of Biomedical Engineering, University of Houston, Houston, TX, USA*

Abstract. Chemical mapping of molecules adsorbed on plasmonic nanostructures is a powerful technique for biomolecular sensing, surface chemistry and plasmon–matter interactions. DC-sputtered gold nanoisland (GNI) substrates have attracted significant attention recently due to its excellent plasmonic enhancement, structural stability and simple fabrication. We provide multimodal characterization of GNI morphological evolution by correlating data obtained from scanning electron microscopy (SEM), localized surface plasmon resonance (LSPR) extinction spectroscopy and surface-enhanced Raman scattering (SERS) microscopy. A rigorous determination of the SERS enhancement factor for benzenethiol self-assembled monolayers on evolving GNI substrates is presented. Rapid statistical analysis shows excellent large-area SERS uniformity by hyperspectral Raman imaging systems based on active-illumination which enables parsimonious sampling of only 2.7% area of the field of view, greatly improving sampling efficiency.

Keywords: Plasmonic nanostructures, surface-enhanced Raman scattering (SERS), Raman spectroscopy and microscopy, vibrational spectroscopy

1. Introduction

Rapid chemical analysis of molecular adsorbates on plasmonic nanostructures is a powerful technique in biomolecular sensing and in the study of surface chemistry and plasmon–matter interactions. Due to either surface plasmon resonance (SPR) or localized surface plasmon resonance (LSPR), optical energy can be coupled into either propagating or non-propagating electron oscillation, respectively. Therefore, both SPR and LSPR can be conveniently investigated by extinction spectroscopy in the transmission configuration [2]. Besides optical extinction, plasmonic resonance also produces highly localized electromagnetic field enhancement near the surface of metallic nanostructures, which subsequently enhances fluorescence and Raman scattering of nearby surface adsorbates [22,39]. Raman spectroscopy is a versatile technique for compositional analysis via inelastic light scattering due to molecular vibrations [3,12,33,34,36,43]. It is particularly suitable for the study of thin surface adsorbates on plasmonic nanostructures via surface-enhanced Raman scattering (SERS) for its high sensitivity, specificity and non-photobleaching property [23,41].

Among various plasmonic nanostructures, metallic nanoislands have been studied as early as in the 1980s [10,38–40], while new substrates have continued to emerge [13,14,16,27,30,44]. The SERS activity of gold nanoisland (GNI) fabricated by a slow deposition process was first observed by Maya [18].

*Corresponding author. E-mail: wshih@uh.edu.

Subsequently Rubinstein et al. carried out a series of studies on plasmonic properties of *evaporated* GNI which were shown to be "metastable" even at room temperature [7,11,37]. Merlen et al. carried out a series of studies [20,21] on *sputtered* GNI with significantly higher deposition rate compared to the work by Maya. They further employed GNI to analyze compounds such as dye molecules which exhibit resonance or pre-resonance effects near the absorption wavelength. More recently, GNI structures were employed in plasmon-enhanced catalysis for decomposition of methyl orange and splitting of water [15,24]. It appears that sputtered GNI provides much better structural and environmental stability for practical applications. Therefore, we are interested in further characterizing its plasmonic properties for SERS applications.

In this paper, we provide multimodal characterization of GNI with respect to different deposition time. We correlate GNI morphological evolution imaged by scanning electron microscopy (SEM), LSPR spectra by extinction spectroscopy and SERS spectra by hyperspectral Raman microscopy [26,28,29,36]. We report systematic determination of the magnitude and spatial uniformity of SERS activity on GNI substrates. We also report, for the first time, a rigorous determination of the SERS enhancement factor (EF) for benzenethiol self-assembled monolayers, a commonly used marker for performance evaluation across various SERS substrates. Further, we demonstrate a parsimonious sampling scheme for large-area SERS mapping enabled by a hyperspectral Raman imaging system based on active-illumination. Finally, we compare image statistics obtained from parsimonious sampling to those from full-coverage sampling.

2. Material and methods

2.1. DC-sputtered gold nanoislands

GNIs were deposited on glass coverslip in a 2″ DC-diode sputtering system (Anatech/Technics "Hummer") with a gold foil target of 99.99% purity. Sputtering conditions were as follows: (a) 10 mA current, 100 mTorr Ar pressure and 25 mm target-to-substrate distance. No. 1 coverslips (VWR Scientific Products) were first immersed in piranha solution (3 : 1 mixture of 98% H_2SO_4 and H_2O_2) for 30 min to remove any organic residue. The cleaned coverslips were then rinsed in DI water and blow-dried with nitrogen before sputtering.

2.2. Hyperspectral Raman imaging systems

We have employed two parallel, hyperspectral imaging systems, line-scan and active-illumination, to characterize the SERS EF and uniformity of GNI substrates. We chose to use the 785 nm output of a CW titanium:sapphire laser (Spectra-Physics 3900S, Spectra-Physics) pumped by a diode-pumped solid state laser (Millennia 10X, Spectra-Physics). In the active-illumination scheme, the laser output was expanded and modulated by a liquid crystal phase spatial light modulator (SLM, LCOS Hamamatsu) into multiple micro-spots at the sample plane in an inverted microscope. The SERS signals excited at these spots were imaged to a slit-less grating spectrograph (SP2300, Princeton Instruments) and simultaneously recorded by a CCD camera (PIXIS 400BR, Princeton Instruments).

In the line-scan scheme, the output from laser was transformed to a uniform line by a Powell lens and two cylindrical lenses. This line was relayed to the side-port and entered an inverted microscope. A galvanometric mirror (GVS011, Thorlabs) was employed to scan and de-scan the line in the transverse direction. The SERS signals excited from the laser line were imaged to the entrance slit of a spectrograph

(LS785, Princeton Instruments) with a CCD detector (PIXIS 400BR, Princeton Instruments) [26,28, 29].

2.3. UV-Vis extinction spectroscopy

A Cray 50 Scan UV-Visible spectrometer (Varian Inc.) was used to measure the UV-Vis spectra from 250 to 1100 nm. A spectrum from a clean coverslip was acquired as the reference and subtracted from raw data. The UV-Vis spectra presented below were averaged from five measurements.

2.4. Benzenethiol self-assembled monolayer

Benzenethiol (BT) was employed as the SERS marker for its ability to form a self-assembled monolayer (SAM) on gold. Briefly, we incubated the GNI substrates in 5 mM benzenethiol (99.9%, Sigma-Aldrich) dissolved in ethanol for 30 min, followed by rinse in pure ethanol for 1 min and nitrogen dry [1]. Using benzenethiol SAM for the quantitative determination of SERS enhancement factor (EF) is advantageous because its surface density on gold is well known, thus enabling an accurate quantification of number of molecules. The choice of the laser wavelength (785 nm) avoids any resonant or pre-resonant effect due to the weak absorption by BT molecules. SERS EF was estimated by comparing to normal Raman signals obtained from neat BT solutions contained in a cell with known volume. SERS EF was alternatively estimated by comparing to a commercial substrate (Klarite, Renishaw Diagnostics Ltd.) with a specification of 1 million EF for BT. No attempt has been made to address the differences between the surface roughness or effective surface area of Klarite, which would be larger than its geometrical projection area. Thus, the SERS EF thus obtained would have inherit uncertainties in these aspects.

3. Results and discussion

3.1. DC-sputtered gold nanoislands (GNI)

The deposition rate of the sputtering machine was first calibrated by coating a gold layer on silicon for 300 s. An SEM image of the cross-section showed that the thickness of the film was $\sim$27 nm. Thus, the average deposition rate was determined to be 0.09 nm/s. Since the GNIs are isolated units, it is not suitable to estimate thickness simply by multiplying the average rate with deposition time. Instead, we use the deposition time to distinguish our samples.

Figure 1(a)–(e) show the SEM images of GNI substrates prepared by 52, 104, 156, 208 and 260 s of deposition, respectively. We analyzed the size of the islands from the SEM images via ImageJ (NIH) by first trimming the SEM images to the same size and smoothed the image twice using a 3×3 moving average filter. We then binarized the images and performed watershed process to separate the connected objects to isolated particles. The processed images are shown in the inset of each image in Fig. 1(a)–(e). Average radii of GNI measured in these images are shown in Fig. 1(f) with each data set fitted by Gaussian distribution with $\mu = 3.36$, 4.20, 4.95, 6.06 and 6.00, and $\sigma = 0.90$, 0.94, 1.20, 1.71 and 1.78, respectively. We observed an increase of GNI radius from 52 to 208 s substrates. However, the growth of nanoisland size stopped after the 208 s sample when additional fine structures began to form on existing nanoislands.

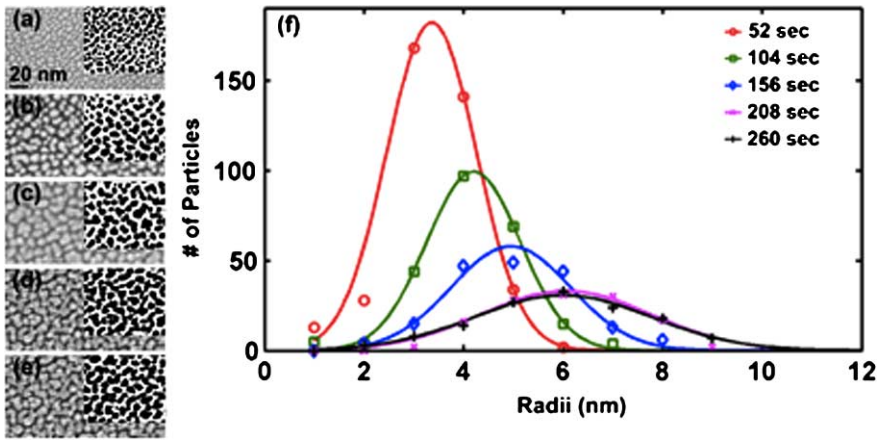

Fig. 1. SEM images of GNI substrates with various deposition time: (a) 52 s, (b) 104 s, (c) 156 s, (d) 208 s and (e) 260 s; (f) corresponding GNI size distribution. (Colors are visible in the online version of the article; http://dx.doi.org/10.3233/BSI-140100.)

4. UV-Vis extinction spectroscopy

As shown in Fig. 2, we measured the UV-Vis spectra of GNI substrates in ambient environment of air ($n = 1$), water ($n = 1.333$), ethanol ($n = 1.362$) and toluene ($n = 1.492$). First of all, unlike in previous reports, our GNIs were stable in various solvents. One characteristic LSPR band ("$*$") was observed in all GNI samples in air, which shifted from 690 to 1100 nm as the deposition time increased (see Fig. 2(a)). A new LSPR band ("$\times$") at $\sim$620 nm emerged after the deposition time reached 156 s, and shifted to 660 nm in the 208 s sample. Similar behavior was also found in extinction spectra measured in other media. However, 156 s, 208 s and 260 s samples showed a clearer band at $\sim$650 nm in higher refractive index media, agreeing with the literature [4,17]. This observation is consistent with the size analysis of nanoislands discussed earlier. The nanostructural changes due to size variations are reflected in the plasmonic resonance. With a short sputtering time, the GNIs were small, and appeared isolated from each other. As the deposition time increased, these isolated islands grew and thus caused the LSPR band to redshift of from 690 nm to 1100 nm. The 156 s sample entered a transition stage: as the deposition time further increased, the bases of the nanoislands began to coalesce, resulting in the new LSPR band. We also observed stronger extinction with increased deposition time, which might also contribute to a larger SERS EF besides the redshift.

5. SERS enhancement factor of GNI substrates

We have characterized the SERS enhancement of GNI substrates using the line-scan and active-illumination Raman systems. GNI substrates coated with benzenethiol SAM were mapped 10 to 20 times at random location across a 22×22 mm^2 area. The average spectra over an area of six 100×100 μm^2 are presented in Fig. 3 after automated curvature correction and background removal [25,32]. Among the major SERS bands observed in all GNI substrates, we selected to study 1075 cm^{-1} (CCC stretch, CS bending) and 1575 cm^{-1} (CC stretching), as marked by asterisk and triangle, respectively. The inset figure shows the dependence of SERS intensity on the deposition time, exhibiting an upward increasing trend. The average SERS intensity of 260 s GNI at 1075 cm^{-1} and 1575 cm^{-1} band were 50.7 and 54.5 times larger than that of 52 s GNI, respectively. This implies the EF is very sensitive to GNI size.

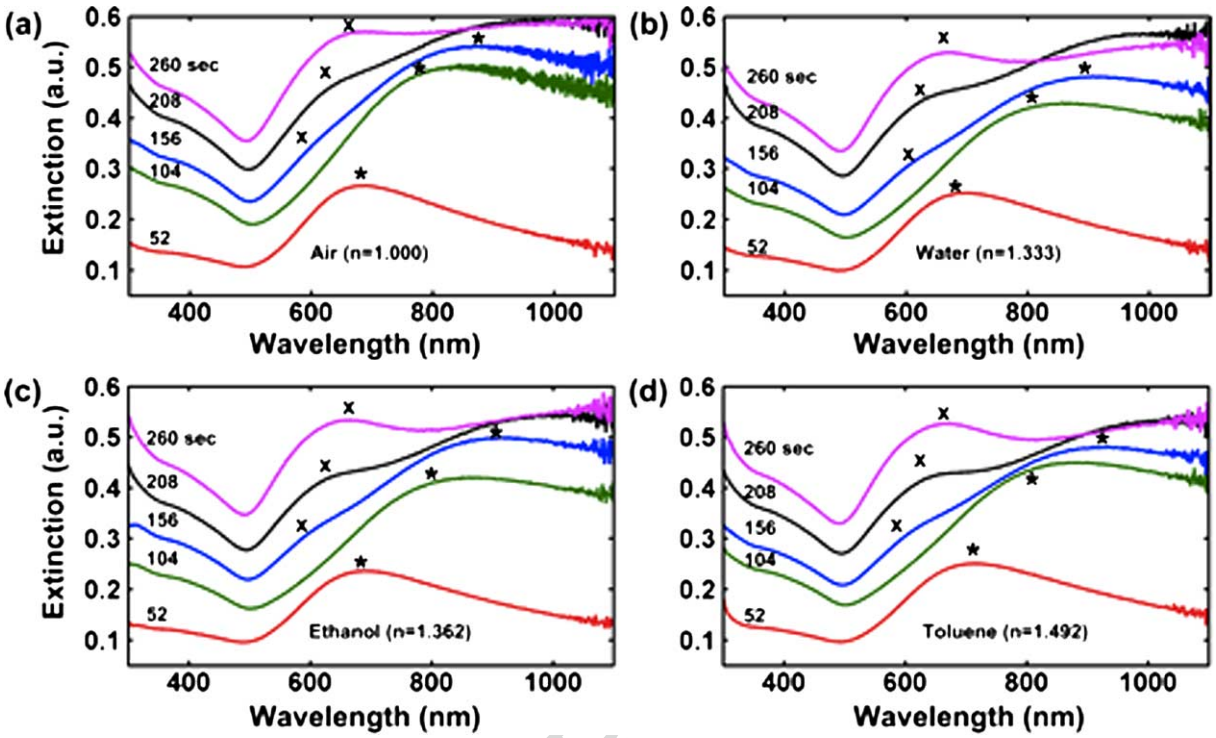

Fig. 2. UV-Vis spectra of GNI of various deposition time in different refractive index media: (a) air, (b) water, (c) ethanol and (d) toluene. (Colors are visible in the online version of the article; http://dx.doi.org/10.3233/BSI-140100.)

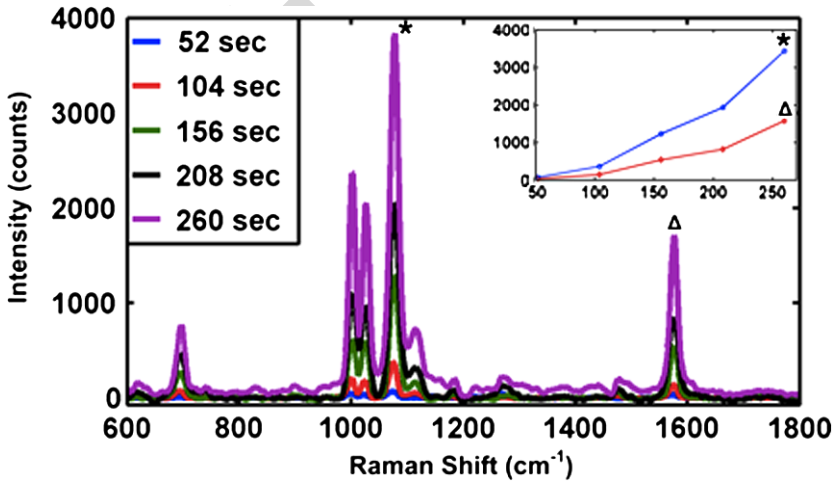

Fig. 3. SERS spectra of benzenethiol SAM coated GNI substrates and dependence of SERS intensity on deposition time in the inset. (Colors are visible in the online version of the article; http://dx.doi.org/10.3233/BSI-140100.)

By comparing to the normal Raman intensity from neat benzenethiol, the EF was $\sim 5.2 \times 10^6$. By comparing the 1575 cm^{-1} band from 260 s GNI and Klarite, we obtained an average of 2.2 times larger SERS intensity from GNI. Since the EF of Klarite is specified at least 1.0×10^6 for benzenethiol SAM, the EF of 260 s GNI was at least $\sim 2.2 \times 10^6$, in-line with the other value.

5.1. Characterization of SERS uniformity using hyperspectral Raman imaging

Confocal Raman microscope has been used to characterize the uniformity of plasmonic substrates [8,42]. An alternative strategy to improve imaging speed is to employ parallel acquisition to obtain hyperspectral data, i.e., images consisting of both a spatial and a spectral dimension, e.g., (x, y, λ) in each camera shot. In Raman microscopy, parallelism has been implemented by global illumination [5,31]. line-scan [6,9,29] and active-illumination [19,26,28]. Global illumination uses tunable narrow-band filters and wide-field image collection to acquire a Raman map by sequentially scanning through multiple wavelengths. This is very time-consuming because out-of-band Raman photons are blocked by the filter in each scanning step. Moreover, global illumination does not allow the acquisition of hyperspectral data in a single camera shot, rather, it is limited to a "narrow band" image. In contrast, line-scan and active-illumination are truly parallel, hyperspectral acquisition schemes with substantial throughput advantages. In a typical line-scan system, the laser is shaped into a long line and focused onto the sample while the entire line is imaged to the spectrograph entrance slit. Thus, spatially-resolved spectra along the entire line can be recorded in a single camera snapshot. An active-illumination system, however, splits the laser into a semi-arbitrary pattern of micro-spots at the sample and collects the Raman spectra from all spots simultaneously in a single camera snapshot. An important advantage of active illumination over the line-scan approach is that semi-random parsimonious sampling in a 2-dimensional plane can be employed to construct unbiased, representative statistics efficiently.

Here we have employed the active-illumination system to characterize SERS uniformity on the 208 s GNI substrate. Each illumination pattern contained 62 laser spots with randomly selected spatial positions. A reference measurement from silicon wafer was recorded for intensity calibration of each pattern. Figure 4(a)–(e) show hyperspectral images acquired using five illumination patterns with background removed by a 5th order polynomial and intensity calibration [26,35]. Figure 4(f) shows the average SERS spectrum (red curve) with ± 1 standard deviation (gray shade). Similar data collected by the line-scan system are also presented in Fig. 4(f), indicating the same major SERS bands and peak ratios were obtained by the active-illumination and line-scan systems. The overall mean and standard deviation of the SERS intensity from the 310 spots in 5 illumination patterns were $8.08 \times 10^4 \pm 6.26\%$, which agree well with those obtained from the line-scan system ($7.86 \times 10^4 \pm 5.92\%$). The comparison suggests that parsimonious semi-random sampling of only $\sim 2.7\%$ sample area can captures unbiased, representative statistics similar to those obtained by 100% sampling. Therefore, the sparse-sampling scheme can provide a highly efficient way to collect data from SERS substrates for the extraction of representative statistics.

SERS maps are generated using the BT SERS bands at ~ 1075 cm^{-1} and ~ 1575 cm^{-1}, as shown in Fig. 5(a) and (b), respectively, based on a total of 310 spots that corresponding to $\sim 2.7\%$ fill-factor of the total field of view. The mean and standard deviation of SERS intensities measured from each illumination pattern was $7.60 \times 10^4 \pm 6.72\%$, $8.41 \times 10^4 \pm 4.11\%$, $8.11 \times 10^4 \pm 6.62\%$, $8.46 \times 10^4 \pm 7.75\%$ and $7.82 \times 10^4 \pm 6.12\%$.

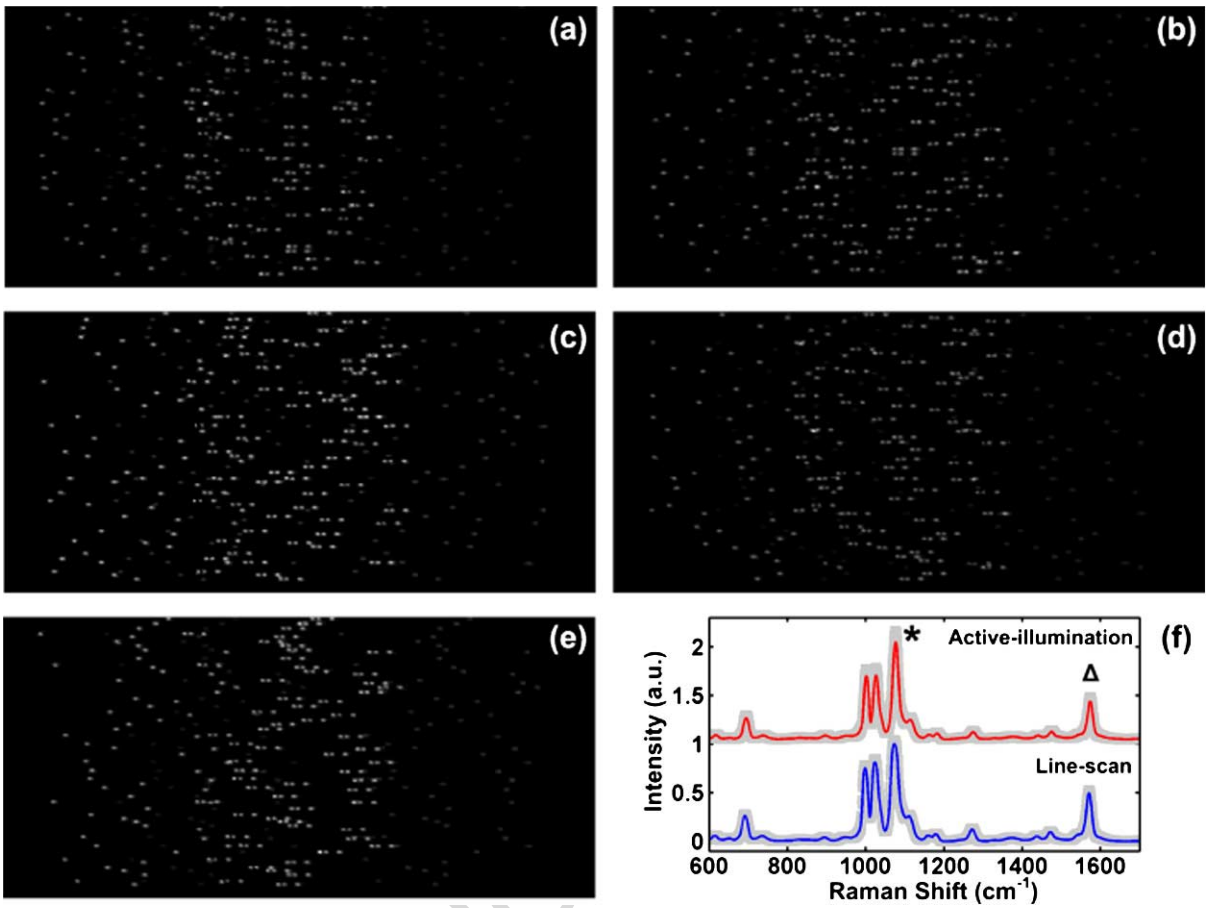

Fig. 4. Hyperspectral SERS images and spectra: (a)–(e) raw CCD images acquired using individual illumination patterns; (f) average SERS spectra from the active-illumination system and line-scan system with ± 1 standard deviation (gray shade). (The colors are visible in the online version of the article; http://dx.doi.org/10.3233/BSI-140100.)

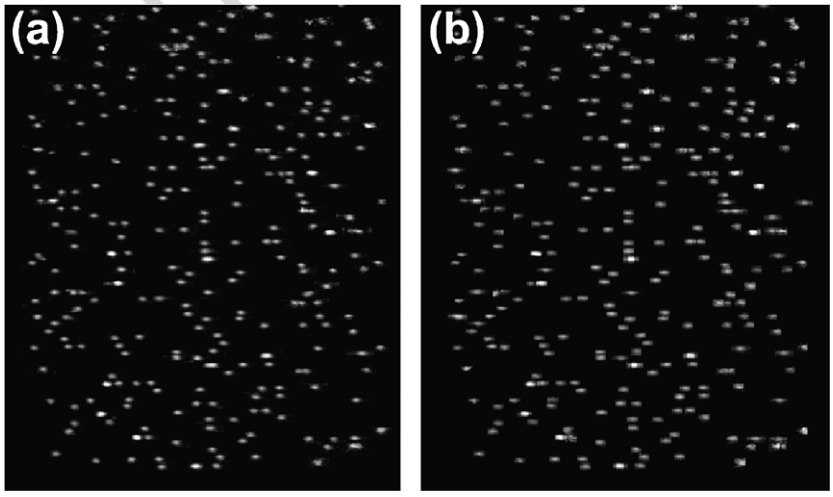

Fig. 5. SERS maps of benzenethiol SAM using two peaks: (a) 1075 cm^{-1} and (b) 1575 cm^{-1}.

6. Conclusions

In summary, we have demonstrated DC-sputtered gold nanoislands provide a low-cost, uniform SERS substrate with an enhancement factor comparable to commercial substrates. By correlating SEM, extinction spectroscopy, and SERS microscopy, GNI's plasmonic behavior has been investigated with respect to morphological changes as deposition time increased, as well as ambient environmental changes. The UV-VIS extinction spectra showed a stronger extinction for GNI samples prepared by longer deposition time. SERS performance has been characterized using benzenethiol self-assembled monolayer as the marker. The enhancement factor of GNIs increased with deposition time and the value for 260 s was $\sim 5.2 \times 10^6$. Large-area SERS uniformity has been evaluated by two hyperspectral Raman imaging systems, active-illumination and line-scan, over randomly selected locations. The overall SERS intensity statistics were $8.08 \times 10^4 \pm 6.26\%$ and $7.86 \times 10^4 \pm 5.92\%$ using the active-illumination and the line-scan systems, respectively. The results suggest our parsimonious sampling scheme using active-illumination can obtain representative, unbiased statistics even when the total sampling area is only 2.7% of the entire field of view.

Acknowledgements

WCS acknowledges funding from National Science Foundation (NSF) CAREER Award (CBET-1151154), National Aeronautics and Space Administration (NASA) Early Career Faculty Grant (NNX12AQ44G), and Gulf of Mexico Research Initiative (GoMRI-030).

References

[1] M.E. Abdelsalam, P.N. Bartlett, J.J. Baumberg, S. Cintra, T.A. Kelf and A.E. Russell, *Electrochemistry Communications* **7** (2005), 740–744.
[2] J.N. Anker, W.P. Hall, O. Lyandres, N.C. Shah, J. Zhao and R.P. Van Duyne, *Nature Materials* **7** (2008), 442–453.
[3] K.L. Bechtel, W.C. Shih and M.S. Feld, *Optics Express* **16** (2008), 12737–12745.
[4] B. Brian, B. Sepulveda, Y. Alaverdyan, L.M. Lechuga and M. Kall, *Optics Express* **17** (2009), 2015–2023.
[5] J.M. Chalmers and P.R. Griffiths (eds), *Handbook of Vibrational Spectroscopy*, Vols 1–5, Wiley, Chichester, 2002.
[6] K.A. Christensen and M.D. Morris, *Applied Spectroscopy* **52** (1998), 1145–1147.
[7] I. Doron-Mor, H. Cohen, Z. Barkay, A. Shanzer, A. Vaskevich and I. Rubinstein, *Chemistry* **11** (2005), 5555–5562.
[8] M.R. Gartia, Z. Xu, E. Behymer, H. Nguyen, J.A. Britten, C. Larson, R. Miles, M. Bora, A.S. Chang, T.C. Bond and G.L. Liu, *Nanotechnology* **21** (2010), 395701.
[9] K. Hamada, K. Fujita, N. Isaac Smith, M. Kobayashi, Y. Inouye et al., *J. Biomed. Opt.* **13**(4) (2008), 044027.
[10] C. Jennings, R. Aroca, A.M. Hor and R.O. Loutfy, *Analytical Chemistry* **56** (1984), 2033–2035.
[11] G. Kalyuzhny, A. Vaskevich, G. Ashkenasy, A. Shanzer and I. Rubinstein, *Journal of Physical Chemistry B* **104** (2000), 8238–8244.
[12] C. Krafft, S. Dochow, I. Latka, B. Dietzek and J. Popp, *Biomedical Spectroscopy and Imaging* **1** (2012), 39–55.
[13] M. Li, J. Lu, J. Qi, F. Zhao, J. Zeng, J.C.-C. Yu and W.-C. Shih, *Journal of Biomedical Optics* **19** (2014), 050501.
[14] M. Li, F. Zhao, J. Zeng, J. Qi, J. Lu and W.-C. Shih, *Journal of Biomedical Optics* **19** (2014), 111611.
[15] Z.W. Liu, W.B. Hou, P. Pavaskar, M. Aykol and S.B. Cronin, *Nano Letters* **11** (2011), 1111–1116.
[16] T. López-Luke, D.A. Wheeler, E. de la Rosa, A. Torres-Castro, S.A. Adams, L.S. Zavodivker and J.Z. Zhang, *Biomedical Spectroscopy and Imaging* **1** (2012), 275–291.
[17] M.D. Malinsky, K.L. Kelly, G.C. Schatz and R.P. Van Duyne, *Journal of the American Chemical Society* **123** (2001), 1471–1482.
[18] L. Maya, *Journal of Vacuum Science & Technology A: Vacuum, Surfaces, and Films* **15** (1997), 238.
[19] S.T. McCain, M.E. Gehm, Y. Wang, N.P. Pitsianis and D.J. Brady, *Applied Spectroscopy* **60** (2006), 663–671.
[20] A. Merlen, V. Gadenne, J. Romann, V. Chevallier, L. Patrone and J.C. Valmalette, *Nanotechnology* **20** (2009), 215705.
[21] A. Merlen, F. Lagugne-Labarthet and E. Harte, *Journal of Physical Chemistry C* **114** (2010), 12878–12884.

[22] M. Moskovits, *Reviews of Modern Physics* **57** (1985), 783–826.
[23] M. Moskovits, *Journal of Raman Spectroscopy* **36** (2005), 485–496.
[24] P. Pavaskar, J. Theiss and S.B. Cronin, *Optics Express* **20** (2012), 14656–14662.
[25] J. Qi, K.L. Bechtel and W.-C. Shih, *Biomedical Spectroscopy and Imaging* **3** (2014), 359–368.
[26] J. Qi, J. Li and W.-C. Shih, *Biomedical Optics Express* **4** (2013), 2376–2382.
[27] J. Qi, P. Motwani, M. Gheewala, C. Brennan, J.C. Wolfe and W.-C. Shih, *Nanoscale* **5** (2013), 4105–4109.
[28] J. Qi and W.-C. Shih, *Optics Letters* **37** (2012), 1289–1291.
[29] J. Qi and W.C. Shih, *Applied Optics* **53** (2014), 2881–2885.
[30] J. Qi, J. Zeng, F. Zhao, S.H. Lin, B. Raja, U. Strych, R.C. Willson and W.-C. Shih, *Nanoscale* **6** (2014), 8521–8526.
[31] S. Schlucker, M.D. Schaeberle, S.W. Huffman and I.W. Levin, *Analytical Chemistry* **75** (2003), 4312–4318.
[32] W.-C. Shih, K. Bechtel and M. Feld, *In Vivo Glucose Measurements*, Wiley, 2009.
[33] W.C. Shih, K.L. Bechtel and M.S. Feld, *Analytical Chemistry* **79** (2007), 234–239.
[34] W.C. Shih, K.L. Bechtel and M.S. Feld, *Optics Express* **16** (2008), 12726–12736.
[35] W.C. Shih, K.L. Bechtel and M.S. Feld, *Handbook of Optical Sensing of Glucose in Biological Fluids and Tissues*, CRC Press, 2008.
[36] N. Sudheendran, J. Qi, E. Young, A. Lazar, D. Lev, R. Pollock, K. Larin and W.-C. Shih, *Laser Physics Letters* **11** (2014), 105602.
[37] A.B. Tesler, B.M. Maoz, Y. Feldman, A. Vaskevich and I. Rubinstein, *The Journal of Physical Chemistry C* **117** (2013), 11337–11346.
[38] R.P. Vanduyne, J.C. Hulteen and D.A. Treichel, *Journal of Chemical Physics* **99** (1993), 2101–2115.
[39] T. Vo-Dinh, *Trac-Trends in Analytical Chemistry* **17** (1998), 557–582.
[40] E. Vogel, W. Kiefer, V. Deckert and D. Zeisel, *Journal of Raman Spectroscopy* **29** (1998), 693–702.
[41] K.A. Willets and R.P. Van Duyne, *Annual Review of Physical Chemistry* **58** (2007), 267–297.
[42] C.Y. Wu, C.C. Huang, J.S. Jhang, A.C. Liu, C.C. Chiang, M.L. Hsieh, P.J. Huang, D.T. Le, Q.M. Le, T.S. Yang, L.K. Chau, H.C. Kan and C.C. Hsu, *Optics Express* **17** (2009), 21522–21529.
[43] J. Zeng, J. Qi, F. Bai, J.C. Chung Yu and W.-C. Shih, *Analyst* **139** (2014), 4270–4278.
[44] F. Zhao, J. Zeng, M.M.P. Arnob, P. Sun, J. Qi, P. Motwani, M. Gheewala, C.-H. Li, U. Strych, A. Paterson, B. Raja, R. Willson, J.C. Wolfe, T.R. Lee and W.-C. Shih, *Nanoscale* **6** (2014), 8199–8207.